Controlled modification of single colloidal CdSe/ZnS nanocrystal fluorescence through interactions with a gold surface

Céline Vion, Piernicola Spinicelli, Laurent Coolen, Catherine Schwob, Jean-Marc Frigerio, Jean-Pierre Hermier, Agnès Maître

▶ **To cite this version:**

HAL Id: hal-00482758
https://hal.science/hal-00482758

Submitted on 7 Dec 2015

Controlled modification of single colloidal CdSe/ZnS nanocrystal fluorescence through interactions with a gold surface

Céline Vion, Piernicola Spinicelli, Laurent Coolen, Catherine Schwob,
Jean-Marc Frigerio, Jean-Pierre Hermier, Agnès Maître

Controlled modification of single colloidal CdSe/ZnS nanocrystal fluorescence through interactions with a gold surface

Céline Vion[1,2], Piernicola Spinicelli[3], Laurent Coolen[1,2], Catherine Schwob[1,2], Jean-Marc Frigerio[1,2], Jean-Pierre Hermier[3,4], Agnès Maître[1,2]

[1] *Université Pierre et Marie Curie-Paris 6, UMR 7588, INSP, Campus Boucicaut, 140 rue de Lourmel, Paris, F-75015 France*
[2] *CNRS, UMR7588, INSP, Paris, F-75015 France*
[3] *Laboratoire Kastler Brossel, Université Pierre et Marie Curie-Paris 6, École Normale Supérieure, CNRS, CC74, 4 Place Jussieu, 75252 Paris CEDEX 05, France*
[4] *Groupe d'Etude de la Matière Condensée, UFR de Sciences de l'Université de Versailles-Saint-Quentin-en-Yvelines, 45 avenue des Etats-Unis, 78035 Versailles, France.*

agnes.maitre@insp.jussieu.fr

Abstract: Single colloidal CdSe/ZnS nanocrystals are deposited at various distances from a gold film in order to improve their performance as single-photon sources. Photon antibunching is demonstrated and the experimental curves are accurately fitted by theoretical equations. Emission lifetime and intensity are measured and found in excellent agreement with theoretical values. The various effects of a neighbouring gold film are discussed : interferences of the excitation beam, interferences of the fluorescence light, opening of plasmon and lossy-surface-wave modes, modification of the radiation pattern leading to a modified objective collection efficiency. At 80 nm from the gold film, when using an objective with 0.75 numerical aperture, about a 2.4-fold increase of the detected intensity is evidenced.

OCIS codes: (270.5290) Photon statistics ; (240.6680) Surface plasmons.

References

1. B. C. Buchler, T. Kalkbrenner, C. Hettich and V. Sandoghdar, "Measuring the quantum efficiency of the optical emission of single radiating dipoles using a scanning mirror", Phys. Rev. Lett. **95**, 063003 (2005).
2. X. Brokmann, L. Coolen, M. Dahan and J.-P. Hermier, "Measurement of the radiative and nonradiative decay rates of single CdSe nanocrystals through a controlled modification of their spontaneous emission", Phys. Rev. Lett. **93**, 107403 (2004).
3. M. D. Leistikow, J. Johansen, A. J. Kettelarij, P. Lodahl and W. L. Vos, "Size-dependent oscillator strength and quantum efficiency of CdSe quantum dots controlled via the local density of states", Phys. Rev. B **79**, 045301 (2009).
4. W. L. Barnes, "Fluorescence near interfaces: the role of photonic mode density", J. Mod. Opt. **45**, 661 (1998).
5. F. D. Stefani, K. Vasilev, N. Bocchio, N. Stoyanova and M. Kreiter, "Surface-plasmon-mediated single-molecule fluorescence through a thin metallic film", Phys. Rev. Lett. **94**, 023005 (2005).
6. K. Ray, R. Badugu and J. R. Lakowicz, "Metal-enhanced fluorescence from CdTe nanocrystals : A single-molecule fluorescence study", J.Am.Chem.Soc. **128**, 8998 (2006).
7. X. Wu, Y. Sun and M. Pelton, "Recombination rates for single colloidal quantum dots near a smooth metal film", Phys. Chem. Chem. Phys. **11**, 5867 (2009).

8. E. Fort and S. Gresillon, "Surface enhanced fluorescence", J. Phys. D **41**, 013001 (2008).
9. K. T. Shimizu, W. K. Woo, B. R. Fisher, H. J. Eisler and M. G. Bawendi, "Surface-enhanced emission from single semiconductor nanocrystals", Phys. Rev. Lett. **89**, 117401 (2002).
10. Ito Yuichi, Matsuda Kazunari and Kanemitsu Yoshihiko, "Mechanism of photoluminescence enhancement in single semiconductor nanocrystals on metal surfaces", Phys. Rev. B **75**, 033309 (2007).
11. E. D. Palik, "Handbook of Optical Constants of Solids", Academic Press (2005).
12. B. Lounis, H. A. Bechtel, D. Gerion, P. Alivisatos and W. E. Moerner, "Photon antibunching in single cdse/zns quantum dot fluorescence", Chem. Phys. Lett. **329**, 399 (2000).
13. P. Michler, A. Kiraz, C. Becher, W. V. Schoenfeld, P. M. Petroff, L. Zhang, E. Hu and A. Imamoglu, "A quantum dot single-photon turnstile device", Science **290**, 2282 (2000).
14. G. Messin, J. P. Hermier, E. Giacobino, P. Desbiolles and M. Dahan, "Bunching and antibunching in the fluorescence of semiconductor nanocrystals", Opt. Lett. **26**, 1891 (2001).
15. R.Hanbury-Brown and R.Q. Twiss, Nature **178**, 1447 (1956).
16. M Nirmal, B. O. Dabbousi, M. G. Bawendi, J. J. Macklin, J. K. Trautman, T. D. Harris and L. E. Brus, "Fluorescence intermittency in single cadmium selenide nanocrystals", Nature **383**, 802 (1996).
17. B. R. Fisher, H.-J. Eisler, N. E. Stott and M. G. Bawendi, "Emission Intensity Dependence and Single-Exponential Behavior In Single Colloidal Quantum Dot Fluorescence Lifetimes", J. Phys. Chem. B **108**, 143-148 (2004).
18. X. Brokmann, E. Giacobino, M. Dahan and J. P. Hermier, "Highly efficient triggered emission of single photons by colloidal cdse/zns nanocrystals", Appl. Phys. Lett. **85**, 712 (2004).
19. S. A. Empedocles, R. Neuhauser and M. G. Bawendi, "Three-dimensional orientation measurements of symmetric single chromophores using polarization microscopy", Nature **399**, 126 (1999).
20. W. Lukosz and R. E. Kunz, "Light emission by magnetic and electric dipoles close to a plane interface. i. total radiated power", J. Opt. Soc. Am., **67** 1607 (1977).
21. R. R. Chance, A. Prock and R. Silbey, "Lifetime of an emitting molecule near a partially reflecting surface", J. Chem. Phys. **60**, 2744 (1974).
22. G. W. Ford and W. H. Weber, "Electromagnetic interactions of molecules with metal surfaces", Phys. Rep. **113**, 195 (1984).
23. W.H.Weber and C.F.Eagen, "Energy transfer from an excited dye molecule to the surface plasmons of an adjacent metal", Opt. Lett. **4**, 236 (1979).
24. K. Ray, H. Szmacinski, J. Enderlein, and J.R. Lakowicz, "Distance dependence of surface plasmon-coupled emission observed using Langmuir-Blodgett films", Appl. Phys. Lett. **90**, 251116 (2007).
25. J. Enderlein, "Single-molecule fluorescence near a metal layer", Chem. Phys. **247**, 1 (1999).
26. C. A. Leatherdale, W.-K. Woo, F. V. Mikulec and M. G. Bawendi, "On the absorption cross section of CdSe nanocrystal quantum dots", J. Phys. Chem. B **106**, 7619 (2002).
27. W. Lukosz, "Theory of optical-environment-dependent spontaneous emission rates for emitters in thin layers", Phys. Rev. B **22**, 3030 (1980).
28. R. T. Holm, S. W. McKnight, E. D. Palik and W. Lukosz, "Interference effects in luminescence studies of thin films", Appl. Opt. **21**, 2512 (1982).

Controlling the spontaneous emission of single nano-emitters such as CdSe/ZnS colloidal nanocrystals is a challenge with implications for many fields such as quantum optics (single-photon generation) and biolabelling (single-particle tracking). Placing an emitter in a controlled environment is a way to modify the local density of photonic states (LDOS) and improve the efficiency of the dipole : excitation, decay rate, quantum yield, collection efficiency... In the last few years an increasing interest has been given to solid state cavity quantum electrodynamics experiments. Coupling epitaxial quantum dots to cavities has shown a strong effect on emission properties.

However the LDOS is also strongly modified in the vicinity of a simple planar interface, allowing enhanced decay rate and improved collection efficiency through radiation redirection. Planar systems have been studied for several decades because they can be prepared with high precision and reproducibility. They proved to be a nearly perfect platform for the quantitative study of photophysical effects such as excitation enhancement, energy redistribution, and quenching. For instance, the well defined modification of the local density of states with distance to a metallic interface has been used to deduce properties of nanocrystals such as their quantum yield and emission dipole type (at single scale) [1, 2] and the oscillator strength (at collective scale) [3].

Close to a metallic interface, the emission of a nanocrystal can be strongly coupled to surface plasmon modes. Spontaneous emission rate enhancement as a function of the distance to a metallic film has been the subject of numerous studies at collective scale [4] and some at single-emitter scale [1, 5, 6, 7], with some applications for imaging [8]. But coupling to plasmons also leads to a strong improvement of non radiative decay channels. Different works addressing single nanocrystal fluorescence directly on a metal surface have reported strong quantum yield reductions [9, 10].

In this article, we study single CdSe/ZnS nanocrystals at different distances from a gold film and analyze their emission decay rates and detected intensities. Our perspective is to control the coupling of a single photon source to a metal interface in order to improve its efficiency.

In order to describe the modifications of a single-photon source as a function of the distance to a gold film, various aspects need to be taken into account : excitation, radiative and non-radiative decays, radiation pattern and collection efficiency. In the first and second section, we respectively describe the sample preparation and prove that our samples constitute single photon sources. In the third section, we measure the excited-state decay rate as a function of the distance to the gold film, and compare it with a theoretical model, distinguishing the radiative and non-radiative contributions. In the last section, we compare the detected fluorescence intensities in the presence and absence of a gold interface, and explain the observed 2.4-fold increase by theoretically considering the various effects on excitation, decay and collection.

1. Samples fabrication

We prepare samples so that single nanocrystals can be observed at a known distance d from a gold film. We separate the nanocrystals from the gold surface with a silica spacer of thickness d deposited on the gold film. In order to compare the measurements with theoretical calculations, the samples must have well-defined geometrical and optical properties (low roughness, known dielectric constants).

A 200 nm-thick gold layer was deposited by thermal evaporation ($\approx 10^{-6}$ torr) on a glass substrate (fig. 1). An atomic-force-microscope image of our gold surface revealed a root-mean-square roughness of less than 2.2 nm. A thin film of SiO_2 was deposited on gold by sputtering with a partial O_2 pressure of 10^{-3} torr. Seven samples were prepared with different values for the silica layer thickness d from 18 nm up to 300 nm. By spectroscopic ellipsometry, d was measured for each sample with 2-nm accuracy, and the dielectric constant of Au was determined in the wavelength range 300-750 nm and found very close to handbook values [11].

CdSe/ZnS core-shell nanocrystals (Invitrogen/QDot, 565 nm peak emission) were spin coated on the silica layer. The density of nanocrystals was chosen very low ($\approx 0.1/\mu m^2$) so that they could be observed at the single-emitter level by standard confocal microscopy. The nanocrystals were covered by a poly(methylmethacrylate) (PMMA) layer of thickness 60 nm (measured by profilometry) in order to protect them from oxidation. The samples were observed either with an air objective (0.75 numerical aperture, 40x) or with an oil-immersion objective (1.4 numerical aperture, 100x), with an index-matching immersion oil of index around 1.5. The silica and PMMA layers have very similar refractive indices ($n_{SiO2} = 1.44$ and $n_{PMMA} = 1.49$ at visible wavelength, measured by ellipsometry), so that we consider them for future calculations as having the same refractive index $n = 1.5$.

2. Single-photon emission

In the perspective of using our device for later quantum optics experiments, we show that single-photon emission, which is a well-known property for these nanocrystals [12, 13, 14], is still
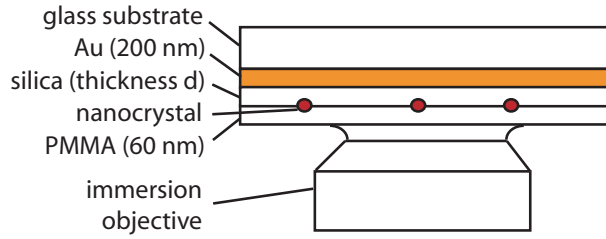
Figure 1. Schematic of the sample and the observation configuration.

present in our samples. This also proves that the single nanocrystals did not aggregate in the sample preparation process.

By use of an immersion objective, a nanocrystal is excited at 400 nm by a pulsed laser diode, with a pulse peak power 2.5 mW, and a pulse duration 80 ps and repetition period $T = 200$ ns. As the typical nanocrystal decay time is 20 ns, much larger than the pulse duration and much shorter than T, only one photon should be emitted per excitation pulse.

We verify this by evidencing photon antibunching on a Hanbury-Brown and Twiss photon correlation setup [15]: the fluorescence signal is separated by a beamsplitter into two beams focused on two avalanche photodiodes in photon-counting regime connected to an acquisition card. The card measures the time intervals τ between one photon detection on one photodiode and the next detection on the other photodiode (negative values of τ are accessed by adding a 400 ns cable delay after the second photodiode), and builds a histogram of the coincidence delays τ which constitutes a measurement of the fluorescence intensity time correlations.
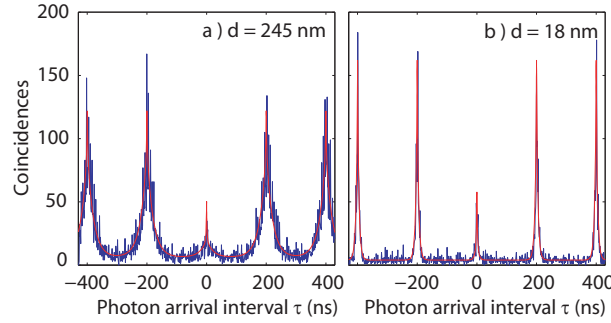
Figure 2. Histogram of the time intervals τ between one photon detection on a photodiode and the next detection on the other photodiode for a nanocrystal at distance $d =$ (a) 256 nm, (b) 18 nm from a gold/silica interface. The red lines are theoretical curves obtained as explained in the text and Appendix.

Figure 2 presents such histograms for gold-nanocrystal distances (a) $d = 256$ nm and (b) 18 nm. We observe series of peaks separated by the laser repetition period T. These peaks correspond to one photon generated by one laser pulse and the next photon generated by another pulse after a time multiple of T. The smaller area of the central correlation peak at $\tau = 0$ is the signature of single-photon emission : two photons are never detected at the same time because photons are emitted one by one, and two photons are never generated by the same laser pulse.

The presence of a residual central peak may be attributed either to incomplete nanocrystal-

emission antibunching (multi-exciton emission) or to bunched background PMMA luminescence. In order to estimate the contribution from multi-excitonic emission, we assume that there is no such contribution (the nanocrystal emission is completely antibunched) and compare the resulting theoretical curve with the experimental data.

We model the measured luminescence on each photodiode by a sum of a nanocrystal signal of the form:

$$I_{NC}(t) = \widetilde{I}_{NC}(t) \sum_n \Gamma T e^{-\Gamma(t-nT)} H(t-nT) \tag{1}$$

and a background signal:

$$B(t) = B_0 + B_P \sum_n \Gamma_P T e^{-\Gamma_P(t-nT)} H(t-nT) \tag{2}$$

where H is the Heaviside function, Γ and Γ_P are respectively the nanocrystal and PMMA excited-state lifetimes, and B_0, B_P and $\widetilde{I}_{NC}(t)$ correspond respectively to the dark counts, PMMA luminescence and nanocrystal luminescence intensities (in photons per sec.), averaged on timescales much larger than T. We take into account the fact that, due to blinking [16] and other effects of local fluctuations [17], the nanocrystal intensity $\widetilde{I}_{NC}$ shows variations in time (on timescales assumed much larger than T). On the other hand, B_0 and B_P are assumed to be constant. From their decay and intensity time trace curves (see Appendix), for each of the two nanocrystals (a) and (b) considered here, we respectively measured $1/\Gamma = 20.5$ and 5 ns, $1/\Gamma_P = 1.5$ ns (in both cases), $B_0 = 1120$ and 800 counts/s, $B_P = 730$ and 400 counts/s, $\langle \widetilde{I}_{NC} \rangle = 5200$ and 2150 counts/s and $\langle \widetilde{I}_{NC}^2 \rangle = 35 \times 10^6$ and 6.2×10^6 (counts/s)^2.

The correlation function formula resulting from eqs 1 and 2, and assuming antibunched nanocrystal emission, is calculated in the Appendix. The theoretical curve is plotted (red line) on fig. 2, using the above parameters which, let us insist, were obtained from independent measurements with no fitting parameter. We find an excellent agreement with the experimental curves: our data are well described by the assumption of nanocrystal single-photon emission. This indicates that the small peak at $\tau = 0$ is entirely caused by the PMMA luminescence, without any contribution from any multi-exciton emission.

We also note that the peak width, which scales as the emission decay time Γ (see eq. 21), is larger on fig. 2(a) than on fig. 2(b). This implies that for the second sample ($d = 18$ nm) the repetition rate of the laser pulses may be increased without overlapping the successive single-photon emissions. In other words, under pulsed excitation, the proximity to a gold film can help to increase the maximum rate of a single-photon source. However, below a certain distance some non-radiative decay channels may be opened, which would damage the overall single-photon emission efficiency.

We detail this point in the next section by giving experimental and theoretical values of the emission decay rate of a nanocrystal at a distance d from a gold film.

3. Emission decay rate

In this section, we measure the excited-state decay rates Γ of individual nanocrystals at different distances d from a gold film. We start by giving a theoretical model for the experiment, and distinguish in Γ the components corresponding to radiative decay, coupling to surface plasmons, or absorption. Then the experimental results are given and compared with the theoretical dependence $\Gamma(d)$.

The experiments were performed using an oil-immersion objective, so that for this section we need to consider an emitter in an infinite dielectric half-space of dielectric constant $\varepsilon_d = 2.25$

(corresponding to the silica, PMMA and immersion oil layers, all having an index 1.5), at a distance d from an interface with a gold half-space of dielectric constant $\varepsilon'_m + i\varepsilon''_m = -7.06 + 1.29i$ (ellipsometric measurement performed at 565 nm). The gold medium is considered semi-infinite, as the gold layer thickness is much larger than the optical absorption length in gold.

We assume that the nanocrystals have no non-radiative decay channel except the ones introduced by the presence of the gold film. Indeed for single nanocrystals on a glass coverslip, the quantum yield is greater than 0.95 [18].

The emission properties (lifetime and emission diagram) strongly depend on the nanocrystal orientation. We take into account the nature of the transition dipole of colloidal nanocrystals, which is 2D-degenerate and located in a plane perpendicular to the crystalline c-axis [18, 19]. The single nanocristal emission can be decomposed into the emission of two perpendicular linear dipoles. Each linear dipole at a distance d from the gold film with an angle δ with the normal to the sample plane (fig. 3(a)) can then be decomposed into its components parallel and perpendicular to the interface : $\Gamma_{1D}^{\delta}(d) = \Gamma_{1D}^{\perp}(d)\cos^2(\delta) + \Gamma_{1D}^{||}(d)\sin^2(\delta)$ [20]. The decay rate of a 2D-degenerate dipole with a c-axis tilted with an angle θ relative to the normal to the sample plane (fig. 3(b)) is then : $\Gamma(\theta, d) = \frac{1}{2}[\Gamma_{1D}^{\perp}(d)\sin^2(\theta) + \Gamma_{1D}^{||}(d)(1 + \cos^2(\theta))]$.
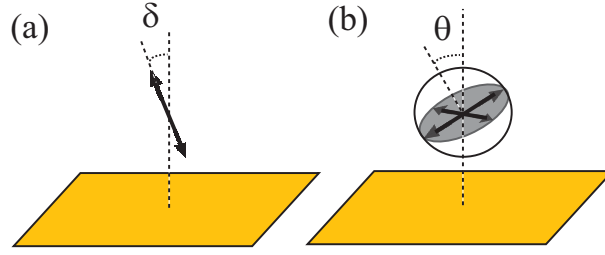

Figure 3. Schematic representation of (a) a linear dipole (arrow), oriented at an angle δ from the normal to the sample plane, and (b) a nanocrystal with crystalline c-axis oriented at an angle θ from the sample plane : the 2D-degenerate emission can be decomposed into two dipoles (indicated by arrows) perpendicular to the c axis.

The decay rates $\Gamma_{1D}^{||}(d)$ and $\Gamma_{1D}^{\perp}(d)$ for linear dipoles were calculated using the semi-classical model of ref. [21, 20], where the excited-state decay rate Γ is taken to be the energy dissipation rate of the classical dipole : for a weakly damped dipole, the relation between dissipated power P and dipole energy $E_{dip.}$ can be expressed as $P = -dE_{dip.}/dt = -\Gamma E_{dip.}$, so that the decay rate can be inferred from the calculation of the energy dissipation. The calculated excited-state decay rates $\Gamma(d)$ of the 2D-degenerate dipole are plotted on fig. 4 as a function of d for values of the nanocrystal c-axis orientation $\theta = 0$ (a) and $\pi/2$ (b).

The wavevector $\vec{k}$ of the emitted field can be decomposed into its longitudinal part k_z orthogonal to the interface and its component parallel to the interface $k_{||}$. Depending on the value of $k_{||}$, a wavevector $\vec{k}$ will contribute either to far-field radiation, or to surface-plasmon modes, or to lossy modes (usually called "lossy surface waves"). The integration of the distribution of radiation over the corresponding vector range gives the power dissipated into each channel [22]. The obtained contributions to Γ, noted respectively Γ_{rad}, Γ_{SP} and Γ_{LSW}, are plotted as a function of d on fig. 4 (a) and (b).

The radiative component of the emission, for which $|\vec{k}| = k_d$ (with $k_d = \sqrt{\varepsilon_d}\omega/c$) and therefore $0 < k_{||} < k_d$, interferes with its reflexion on the gold/dielectric interface. As shown in figure 4(a) and (b), the radiative component in far field oscillates relative to the distance to the
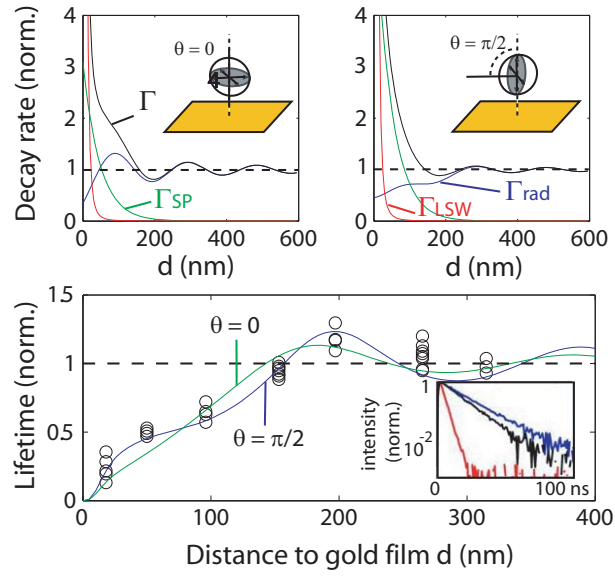
interface with a characteristic period π/k_d.

Figure 4. Theoretical decay rates into each channel : far field radiation Γ_{rad} (blue), surface plasmon mode Γ_{SP} (red), lossy surface waves Γ_{LSW} (green), and total decay rate Γ (black) (normalized to $\Gamma(d = \infty)$) for a nanocrystal with c-axis (a) normal and (b) parallel to the interface. (c) Dots : measured lifetimes $1/\Gamma$ of single CdSe/ZnS nanocrystals, normalized to the lifetime in a homogeneous medium of index 1.5 (18 ns), as a function of the distance d to the gold film. Lines : Calculated theoretical decay rates for a nanocrystal with c-axis normal (green line) and parallel (blue line) to the gold/silica interface. Inset: measured decay curves of three nanocrystals at 18 nm (red), 150 nm (black) and 256 nm (blue) from the gold film. The corresponding fitted decay rates are respectively 3.5, 15.9 and 21.3 ns.

The evanescent part of the dipole emission corresponding to $|\vec{k}| > k_d$ can interact efficiently with the metal only if the dipole is located at a distance much shorter than the wavelength : very close to the interface, the emission near-field component can be coupled into evanescent waves in depth of the metal (in the z direction) while for intermediate distances, it excites mostly the gold surface plasmons. The coupling to surface plasmons is achieved only for a p-polarisation and for $k_{\parallel} = Re(k_{SP})$ where k_{SP} is the wavevector of the surface plasmon polariton (which can be approximated as $k_d\sqrt{\varepsilon'_m(\omega)/(\varepsilon_d(\omega) + \varepsilon'_m(\omega))}$ when $\varepsilon''_m << \varepsilon'_m$). Since $Re(k_{SP}) > k_d$, this coupling can be obtained only in the evanescent wave extension of the near field emitted by the dipole.

Finally, the complex dielectric constant leads to the absorption of all the near-field modes with large $k_{\parallel}$ ($k_{SP} < k_{\parallel} < \infty$).

Experimentally, for each nanocrystal, we recorded the emission decay curve as the histogram of the delays between a laser pulse and the following photon detection (inset of fig. 4(c)). All curves could be fitted by a monoexponential form with a decay rate Γ. The measured emission lifetimes $1/\Gamma$ are plotted in fig. 4(c), as a function of the distance d to the gold film ; several nanocrystals have been considered for each distance d. The given values are normalized to the average lifetime in a homogeneous medium of index $n = 1.5$: 18 ns (measured in toluene).

For a large distance to the gold film, as expected, Γ nears its value in a homogeneous medium

of same index. The lifetime decrease of the CdSe/ZnS nanocrystal in close proximity to the interface (below 100 nm) is consistent with previous reports on coupling to surface plasmon [23, 24, 25]. At 20 nm to the interface a $\approx$7-fold increase of the decay rate is obtained.

We plot on fig. 4(c) the theoretical limit values $1/\Gamma(d, \theta = 0)$ and $1/\Gamma(d, \theta = \pi/2)$ as a function of d. The experimental data are in good agreement with the theoretical curves, within nanocrystal lifetime dispersion (for 20 nanocrystals on a glass coverslip, we found a 10 % dispersion in the measured lifetime values).

As appears on fig. 4(a) and (b), the radiative term Γ_{rad} dominates for distances d larger than 100 nm, and the quantum yield $Y = \Gamma_{rad}/\Gamma$ is close to 1 for large values of d. Oscillations in radiative rate appear due to reflections of the field induced by the dipole back onto the dipole, causing constructive or destructive interferences which either increase or decrease the degenerate dipole's power dissipation. These interferences are more pronounced for the nanocrystal c axis normal to the sample plane, because the emission of a 2D-degenerate dipole is oriented mostly along its c axis (see fig. 7), so that when the c axis is normal to the sample plane more emission is reflected back and interferes with the dipole emission.

The data also show a large decrease in lifetime when the emitter is within 100 nm of the surface. This decrease is interpreted as due to transfer to surface plasmons which occurs when the in-plane wave vector of the incident light is equal to the wave vector of the surface plasmon propagating along the gold/silica interface. The coupling occurs for $k_{\parallel} = Re(k_{SP}) = 1.16k_d$, corresponding to an evanescent mode of wave vector in the z direction $k_z/k_d = \sqrt{1 - (k_{\parallel}/k_d)^2} = 0.59i$. The dipole evanescent mode extension in the dielectric is $1/|k_z| = 104$ nm. Thus, coupling to plasmon modes can be significant and induce spontaneous emission rate modifications only for distances d up to 100 nm, in good agreement with experimental results.

As the fluorophore gets closer to the surface (< 20 nm), the absorption predominates as any evanescent mode ($k > Re(k_{SP})$) emitted by the nanocrystal can be absorbed into the gold layer.

These data show that the emission lifetime may be decreased as much as 7 times by the presence of a gold film, allowing faster single-photon emission. However, the quantum yield is decreased as non-radiative channels Γ_{SP} and Γ_{LSW} are opened, so that not all excitations lead to single-photon emission.

Other aspects should also be taken into account, such as excitation enhancement and emission redirection leading to a better collection. Depending on the desired emission properties, a trade-off must be chosen. The role of all these effects will be developed in the next section.

4. Collection efficiency

Collection efficiency is not crucial when using an immersion objective, as most of the light towards the objective half-space is then collected. However, the use of an immersion objective is limited to situations where the sample can be in contact with the objective. When an air objective needs to be used, for instance when the sample is inside a cryostat or when the emitter is in a specific biological medium, collection efficiency becomes a more important issue. It can then be helpful to tailor the environment of the emitter in order to redirect its emission inside the solid angle of collection of the objective.

In this section we measure the nanocrystal fluorescence intensity when collected by a 40x air objective with 0.75 numerical aperture. We compare the detected intensity from a sample with a gold film at $d = 80$ nm with a reference case where nanocrystals are spin coated on a plain glass coverslip and covered by a 60-nm PMMA layer (see schematics in fig. 5(a) and (b)).

Since the detected intensity turns out to be a much more dispersed quantity than emission decay rate, we choose to perform our measurement on a few hundred nanocrystals for each

sample in order to make a reliable comparison between the two situations. We illuminate the sample area with a Hg lamp with a 425-450 bandpass filter so that the line at 436 nm (of width 3 nm) is selected. The sample is imaged by a CCD camera. Figures 5 (a) and (b) compare the CCD images of the reference sample and the gold sample. Obviously more light is detected from the nanocrystals placed near the gold interface. This is confirmed on fig. 5(c), which plots a histogram of the detected nanocrystal intensities (in photons/sec, averaged over "on" states since nanocrystals blink) from 177 nanocrystals on the gold sample and 300 nanocrystals on the reference sample. An average gain factor of 2.4 in the detected intensity is measured.
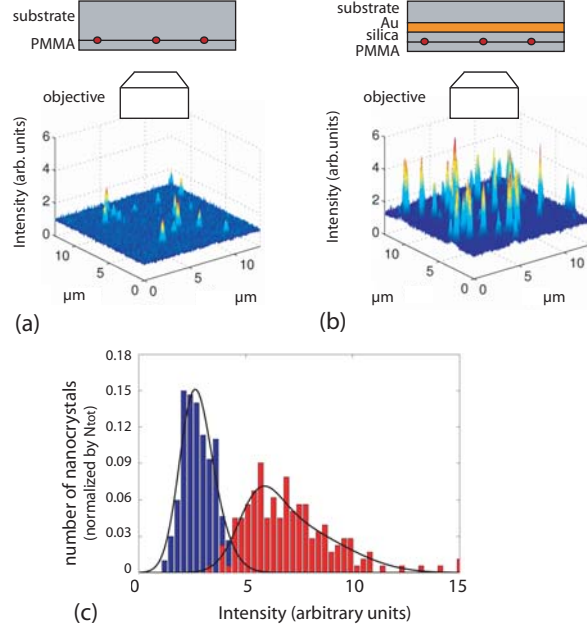

(a)   (b)

(c)

Figure 5. Image measured by CCD camera of a 13x13 μm portion of (a) the reference sample of nanocrystals on glass covered by PMMA and (b) the sample with nanocrystals at $d = 80$ nm from a gold film. (c) Histogram of the detected nanocrystal fluorescence intensities D (in arbitrary units) from the reference sample (red) and the $d = 80$ nm sample (blue). The lines are fits obtained as explained later in the text.

Let us give a theoretical description for these results in order to distinguish the various contributing effects. In order to describe this sample for which no immersion oil was used, we need to include a second air/dielectric interface, at a distance $d + 60$ nm from the gold/dielectric interface.

When using the standard model of a single-photon emitter pumped off-resonance as a two-level system with pumping rate r, radiative decay rate Γ_{rad} and total decay rate Γ, the population of the excited state is $r/(r+\Gamma)$ in the stationary regime, so that one finds a single-photon emission rate :

$$\gamma = r\Gamma_{rad}/(r+\Gamma) \qquad (3)$$

Taking into account the collection efficiency of the objective C and the losses in our optics and the detection efficiency of our camera which we describe as an overall transmission factor

η, we find our experimentally measured quantity, which is the single-photon detection rate (in ph/sec): $D = \gamma C \eta$.

The excitation rate r is related to the excitation power per surface unit P at the nanocrystal location by:

$$r = \frac{\sigma P}{\hbar \omega_{exc}} \tag{4}$$

where $\hbar \omega_{exc}$ is the excitation photon energy and σ is the nanocrystal absorption cross-section. P depends on d because of interferences between incoming and reflected light. Given our incoming excitation $P_0 = 14$W/cm^2 and the typical nanocrystal absorption cross-section $\sigma = 0.1$ nm^2 [12, 26], r is of the order of 2×10^5s^{-1}, much smaller than Γ, so that absorption is the limiting factor in the absorption-emission cycle. The single-photon emission rate in eq. 3 becomes $\gamma \approx rY$, where Y is the nanocrystal quantum yield $\Gamma_{rad.}/\Gamma$. Finally the photon detection rate reduces to:

$$D(d, \theta) = r(d)Y(d, \theta)C(d, \theta)\eta \tag{5}$$

By considering the reflection and transmission coefficients on the sample interfaces, and including the 3-nm linewidth of the excitation spectrum, we plot the excitation power $\beta = r/r_0 = P/P_0$ as a function of d, normalized to the excitation rate $r_0 = \sigma P_0/\hbar \omega_{exc}$ for the nanocrystal in a homogeneous medium of index 1 under the same incoming power per surface unit P_0 (fig. 6(a)). The excitation rate shows large variations as a function of d. At the value $d = 80$ nm, we find an excitation enhancement factor $\beta = 1.29$, as compared to the factor $\beta_{ref} = 0.96$ in the reference sample.

The quantum yield $Y(d)$ is plotted on fig. 6(b) as a function of d, using the calculations presented in the previous section adapted to the case of a two-interfaces system [27]. As explained before, the quantum yield decreases when the nanocrystal is close to the gold film because of non-radiative decay towards surface plasmons or lossy surface waves. This quantum yield must be compared to the quantum yield in the reference sample, which we previously assumed to be $Y_{ref} = 1$.

Profiles of the emission diagrams are plotted on fig. 7 for several nanocrystal environments, using the framework developped in ref. [28] which takes into account the interferences between the direct and the reflected emission. The distance to the gold film has a large effect on the emission diagram, with some configurations ($d = 80$ nm, $d = 250$ nm) more favorable than others ($d = 170$ nm) for collection with a typical air objective. This appears clearly when plotting the ratio $C(d)$ of emission which is collected by an air objective with 0.75 numerical aperture (fig. 6(c)). The value of $C(d)$ is to be compared with its value for the reference sample, respectively 0.09 and 0.06 for vertical and horizontal c-axis.

Eventually, the product βCY is plotted on fig. 8(a), for the gold sample and for the reference sample. At $d = 80$ nm, the presence of the gold film induces a theoretical gain $D/D_{ref} = (\beta CY)/(\beta CY)_{ref}$ of 2.1 and 2.8 for a nanocrystal axis respectively parallel and normal to the film plane. This is coherent with the experimental average gain of 2.4.

In order to actually model the distribution of the experimental values of D in fig. 5(c), we need to include the random distribution of nanocrystal orientations. The number of nanocrystals with c-axis coordinates in the $[\theta, \theta + d\theta; \phi, \phi + d\phi]$ range (ϕ being the azimuth) is:

$$d^2N(\theta, \phi) = N_{tot}\frac{\sin\theta d\theta d\phi}{2\pi} \tag{6}$$

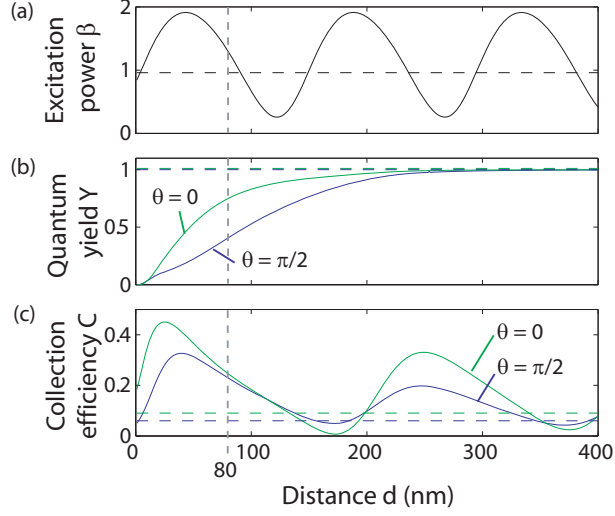where N_{tot} is the total number of nanocrystals considered.

Figure 6. Theoretical influence of the silica spacer thickness d on (a) the normalized excitation surface power β, (b) the quantum yield $Y = \Gamma_{rad.}/\Gamma$ and (c) the collection efficiency C. The curves of (b) and (c) are plotted for a nanocrystal parallel (blue line) and normal (green line) to the sample plane. The values for the reference sample are indicated as dotted lines.

Let us define A as ηr_0. The rate of photon detections is then:

$$D(\theta) = A\beta Y(\theta)C(\theta) \tag{7}$$

so that A depends only on the nanocrystal properties (absorption cross-section σ) and on the excitation (P_0, $\hbar\omega_{exc.}$) and detection (η) conditions, while the geometry of the sample (with or without gold, value of d) is contained only in the dimensionless terms β, Y and C as analyzed previously.

For a realistic description, we need to take into account the dispersion of A from one nanocrystal to the other (corresponding to a dispersion of σ). We assume a gaussian dispersion of width w centered on A_0:

$$G(A) = \frac{1}{\sqrt{2\pi}w} \exp\left(-\frac{(A - A_0)^2}{2w^2}\right) \tag{8}$$

so that, among the $d^2N(\theta,\phi)$ nanocrystals of orientation (θ,ϕ), the number of nanocrystals with a value of A in the range $[A, A + dA]$ is: $d^3N(\theta,\phi,A) = d^2N(\theta,\phi)G(A)dA$. Given eq. 7, the nanocrystals with orientation in the range $[\theta, \theta + d\theta, \phi, \phi + d\phi]$ and photon detection rate in the range $[D, D + dD]$ are the nanocrystals having a value of A in the range $[A, A + dA]$, with $A = D/\beta Y(\theta)C(\theta)$ and $dA = dD/\beta YC$.

Eventually, the number of nanocrystals in a histogram bar D of width dD (which is the quantity that we plot in figure 5(c)) is the sum of nanocrystals of all orientations with the
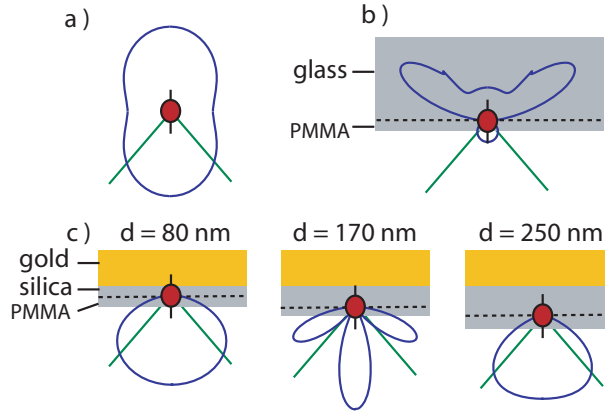
Figure 7. Theoretical emission diagrams (in arbitrary units) of a nanocrystal with vertical c axis ($\theta = 0$), (a) in a homogeneous medium, (b) in the reference sample, and (c) in three gold samples with different values of d (and no immersion oil). The green lines indicate the solid angle which is collected by an air objective with 0.75 numerical aperture.

appropriate A:

$$
\begin{aligned}
dN(D) &= \int_{\theta=0}^{\pi/2} \int_{\phi=0}^{2\pi} d^2 N(\theta,\phi) G\left(\frac{D}{\beta Y(\theta)C(\theta)}\right) \frac{dD}{\beta Y(\theta)C(\theta)} \\
&= N_{tot} dD \int_{\theta=0}^{\pi/2} G\left(\frac{D}{\beta Y(\theta)C(\theta)}\right) \frac{\sin\theta}{\beta Y(\theta)C(\theta)} d\theta
\end{aligned}
\tag{9}
$$

We fit the histograms of figure 5(c) with equation 9, where A_0 and w are the two fitting parameters, characteristic of the nanocrystal sample. The obtained fitted curves are in good agreement with the experimental histograms. The fitting parameters are similar for the two samples, as expected since both samples were made with the same nanocrystal solution: $A_0 = 68$ cts/s and $w = 12$ cts/s for the gold sample, and $A_0 = 61$ cts/s and $w = 16$ cts/s for the reference sample. This confirms that our model provides a complete and appropriate description for the experiment.

Finally, one can use the above calculations to determine which distance d would be the best choice, depending on the situation.

As explained above, when the excitation power is below saturation ($r << \Gamma$), the dependence of the detected intensity on the distance d is given by the product βYC, which is plotted in fig. 8(a). For values of d in the 20-100 and 200-350 nm ranges, the detected intensity is higher than for the reference sample. Maximum gains are obtained at $d = 50$, 220 and 310 nm.

On the other hand, when the excitation power saturates the transition ($r >> \Gamma$), the single-photon emission rate (eq. 3) becomes $\gamma = \Gamma_{rad}$ (in fact, as $\Gamma(d \to 0) = \infty$, for a given r there is a value of d for which $r >> \Gamma$ is no longer true: we neglect this aspect). The detected intensity is then $D = \eta \Gamma_{rad} C$. The excitation power has no effect in this case because the limiting factor in the excitation-emission cycle is the emission. We plot on figure 8(b) the dependence of $\Gamma_{rad} C$ on d. This time, the detected intensity is optimal for $d = 50$ or 250 nm.

However, the detected intensity is not always the best figure of merit. In terms of single-photon emission, a more important aspect may be the possibility to achieve "on-demand" single-photon emission, which means being able to have one photon per excitation pulse. If one assumes that a sufficient pulse power is used to saturate the excitation, the key factor is the probability ηYC for the excited state to recombine into a photon which is detected by the
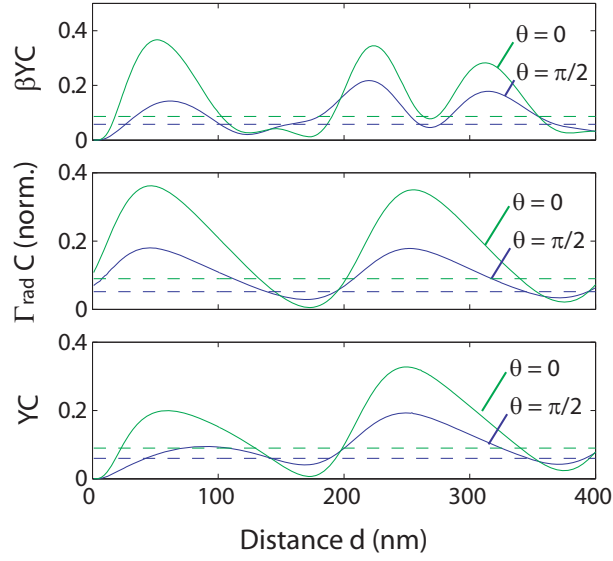
Figure 8. Theoretical plots of the factors (a) βYC, (b) $\Gamma_{rad}C$ (with Γ_{rad} normalized to the decay rate in a homogeneous medium of index $1.5 : 1/18\,\text{ns}$) and (c) YC, which can be used to characterize the quality of a single-photon source (see text).

experimenter. The dependence of YC on d is plotted on fig. 8(c). The best distance is then $d = 250\,\text{nm}$.

Conclusion

We studied here single CdSe/ZnS nanocrystals on a well-characterized sample of gold film and silica spacer. By a careful analysis of background contributions, we evidenced nanocrystal single-photon emission. We measured the effect of the gold film on the emission lifetime and detected intensity, and found an excellent agreement with analytical formulae. Various effects come into play and were analyzed here in fluorescence processes near a metal surface : interferences of the excitation beam, interferences of the emitted light, opening of surface-plasmonic and non-radiative decay channels, emission redirection leading to collection efficiency modification. Depending on the desired parameters of single-photon generation, optimal distances to the gold film were determined. In the case of a non-saturating excitation and an air objective with 0.75 numerical aperture, the excitation power and collection efficiency can be improved, at the expense of a decreased quantum yield. An average enhancement of 2.4 of the single-photon emission rate was measured at 80 nm from the film.

Appendix : Intensity correlation calculation

In this appendix we detail how the theoretical curve for the intensity correlation data on figure 2 was obtained. In a first part we develop the model and calculations leading to the equation for

the intensity correlations of the luminescence signal from a nanocrystal under pulsed excitation, including noise from the PMMA matrix. In a second part we explain how the parameters used in the model were measured experimentally.

The experiment is performed on a Hanbury-Brown and Twiss setup with two photodiodes, and the plotted curve $c(\tau)$ is the histogram of the delays τ between all pairs that can be made with one photon on the first photodiode and one photon on the other photodiode, detected during an overall acquisition time Θ, with a histogram bar width $\delta\tau$. For the measurement of fig. 2, we used the values: $\Theta = 600\,\text{ns}$ and $\delta\tau = 1.2\,\text{ns}$, and $c(\tau)$ was plotted for values from -400 to 400 ns.

When assuming a perfect 50/50 beamsplitter in the system, the luminescence signal $I(t)$ (expressed in counts per second) is the same on both photodiodes. For one photon detected on the first photodiode at time t, the photons on the second photodiode which will contribute to a bar τ of the histogram $c(\tau)$ are the photons that will be detected during the interval $[t + \tau, t + \tau + \delta\tau]$: there are $I(t+\tau)\delta\tau$ such photons. By summing over all photons detected on the first photodiode, we obtain the experimental curve (for $\tau << \Theta$):

$$c(\tau) = \int_{t=0}^{\Theta} I(t)dt I(t+\tau)\delta\tau = \langle I(t)I(t+\tau)\rangle.\Theta.\delta\tau \tag{10}$$

where $\langle\rangle$ is the time-average over the acquisition interval $[0, \Theta]$.

In the total signal $I(t)$ (in counts/sec), we assume a nanocrystal contribution:

$$I_{NC}(t) = \widetilde{I}_{NC}(t) \sum_{n=0}^{\Theta/T} \Gamma T e^{-\Gamma(t-nT)} H(t - nT) \tag{11}$$

where H is the Heaviside function, T is the period of the pulsed laser excitation (here 200 ns), $\widetilde{I}_{NC}(t)$ describes the intensity fluctuations at timescales much larger than T (blinking [16] and fluctuations of the non-radiative channels related to local charge movements [17]), and Γ is the nanocrystal excited-state decay rate (typically 0.05 to 0.15 ns^{-1}).

We add a background signal $B(t)$ with a constant contribution B_0 from the dark counts and room noise and a pulsed contribution from the PMMA luminescence:

$$B(t) = B_0 + B_P \sum_{n=0}^{\Theta/T} \Gamma_P T e^{-\Gamma_P(t-nT)} H(t - nT) \tag{12}$$

where B_P is the (constant) PMMA luminescence intensity averaged over a timescale larger than T, and Γ_P is the PMMA luminescence decay rate (typically 0.5 ns^{-1}).

In order to express $\langle I(t)I(t+\tau)\rangle$, we start with the $\langle B(t)B(t+\tau)\rangle$ term, which may be expressed as:

$$B_0^2 + 2B_0 B_P + \frac{(B_P \Gamma_P T)^2}{\Theta} \sum_{n=0}^{\Theta/T} \sum_{m=0}^{\Theta/T} \int_0^{\Theta} f(t)dt \tag{13}$$

with:
$$f(t) = e^{-\Gamma_P(t-nT)} e^{-\Gamma_P(t+\tau-mT)} H(t + \tau - mT) H(t - nT) \tag{14}$$

For $\tau \leq (m-n)T$,

$$\int_{t=0}^{\Theta} f(t)dt = \int_{mT-\tau}^{\Theta} e^{-2\Gamma_P t} e^{-\Gamma_P \tau} e^{\Gamma_P(n+m)T} dt = \frac{1}{2\Gamma_P} e^{-\Gamma_P((m-n)T-\tau)} \tag{15}$$

and for $\tau \geq (m-n)T$,

$$\int_{t=0}^{\Theta} f(t)dt = \int_{nT}^{\Theta} e^{-2\Gamma_P t}e^{-\Gamma_P \tau}e^{\Gamma_P(n+m)T}dt = \frac{1}{2\Gamma_P}e^{-\Gamma_P(-(m-n)T+\tau)} \tag{16}$$

so that we express $\langle B(t)B(t+\tau)\rangle$ as:

$$B_0^2 + 2B_0 B_P + \frac{(B_P T)^2 \Gamma_P}{2\Theta} \sum_{n=0}^{\Theta/T} \sum_{m=0}^{\Theta/T} e^{-\Gamma_P|\tau-lT|} \tag{17}$$

where $l = m-n$. By a change of variables from (m,n) to (l,k) we write:

$$B_0^2 + 2B_0 B_P + \frac{(B_P T)^2 \Gamma_P}{2\Theta} \sum_{l=-\Theta/T}^{\Theta/T} \sum_{k=-(\Theta/T-l)/2}^{(\Theta/T-l)/2} e^{-\Gamma_P|\tau-lT|} \tag{18}$$

Each $e^{-\Gamma_P|\tau-lT|}$ term corresponds to one peak, centered on $\tau = lT$, as appears on figure 2. Given the chosen interval of values of τ, only the peaks corresponding to values of l ranging from -2 to 2 are observed, so that only these values of l must be considered in order to describe the data. Since $2 \ll \Theta/T$, we obtain:

$$B_0^2 + 2B_0 B_P + \frac{B_P^2 T \Gamma_P}{2} \sum_{l=-2}^{2} e^{-\Gamma_P|\tau-lT|} \tag{19}$$

Similarly, the crossed terms can be obtained:

$$\langle B(t)I_{NC}(t+\tau)+I_{NC}(t)B(t+\tau)\rangle = 2B_0 \left\langle \widetilde{I}_{NC} \right\rangle$$
$$+ B_P \left\langle \widetilde{I}_{NC} \right\rangle \frac{T}{1/\Gamma+1/\Gamma_P} \sum_l \left(e^{-\Gamma_P|\tau-lT|} + e^{-\Gamma|\tau-lT|} \right) \tag{20}$$

where the time-average of the product of $\widetilde{I}_{NC}$ and the exponential term was considered to be the product of the time-average of each, since they vary on two different time scales.

Finally the last term is:

$$\langle I_{NC}(t)I_{NC}(t+\tau)\rangle = \left\langle \widetilde{I}_{NC}^2 \right\rangle \frac{T\Gamma}{2} \sum_{l\neq 0} e^{-\Gamma|\tau-lT|} \tag{21}$$

In this last equation the quantum nature of the nanocrystal emitter has been included by summing only over non-zero values of l: the I_{NC} autocorrelation peak at $\tau = 0$ is removed, as is well known for single-photon emission under pulsed excitation [18].

In the end $\langle I(t)I(t+\tau)\rangle$ is obtained by summing the terms in eq. 19, 20 and 21.

As a second part of this appendix, let us now show that all the necessary parameters can be measured experimentally, independently from the correlation curve which we want to model. The values Θ, $\delta\tau$ and T are set by the experimenter as mentioned above, the missing parameters are Γ, Γ_P, B_0, B_P, $\langle \widetilde{I}_{NC} \rangle$ and $\langle \widetilde{I}_{NC}^2 \rangle$.

We used a Picoquant Timeharp 200 acquisition card, which, in "time-tagged" mode, measures at the same time (i) the delay between one "start" photon on one photodiode and one "stop" photon on the next photodiode with a 1-ns precision, and (ii) the time of each photon pair with a 100 ns precision on an absolute time scale. This allowed us to plot, for the same

acquisition duration, both the correlation curve of interest $c(\tau)$ (histogram of the delays (i)), and the intensity time trace $B_0 + B_P + \widetilde{I}_{NC}(t)$ (square root of the histogram of the times (ii)). Because of nanocrystal blinking, this latter curve shows "on" and "off" states. From the "off" states, the background intensity $B_0 + B_P$ can be obtained. By substracting this background and averaging over the *whole* acquisition duration (not just the "on" states), we obtain $\langle \widetilde{I}_{NC} \rangle$ and $\langle \widetilde{I}_{NC}^2 \rangle$. We find for acquisition (a) $B_0 + B_P = 1850$ counts/s, $\langle \widetilde{I}_{NC} \rangle = 5200$ counts/s and $\langle \widetilde{I}_{NC}^2 \rangle = 35 \times 10^6$ (counts/s)^2, and for acquisition (b) $B_0 + B_P = 1200$ counts/s, $\langle \widetilde{I}_{NC} \rangle = 2150$ counts/s and $\langle \widetilde{I}_{NC}^2 \rangle = 6.2 \times 10^6$ (counts/s)^2. Let us note that, since only the photon pairs with a delay shorter than $4\,\mu$s were recorded, there were just about 40 recorded photon pairs per second, so that the curve $\widetilde{I}_{NC}(t)$ could be plotted with only 1-second resolution on t. Thus in our procedure we neglect the sub-second fluctuations of $\widetilde{I}_{NC}$, an approximation which is quite brutal but eventually seems sufficient to describe our antibunching curves.

After acquiring the data which were used to plot the intensity correlations, we acquired decay curves by using the synchronization pulses from the laser as the "start" input and the photon counts as the "stop" input. By using the "time-tagged" mode, we could also plot the intensity time trace, and distinguish the "on" and "off" part of the acquisition, so that we could plot the decay curve separately for the "off" periods and the "on" periods. For the "off" decay rates, there was an exponentially-decaying component corresponding to the PMMA luminescence (from which the PMMA decay time $1/\Gamma_P$ was obtained) and a constant component corresponding to exterior noise and dark counts. The ratio of the two components yields the value of B_P/B_0. By substracting the decay of the "off" periods from the decay of the "on" period, we isolate the nanocrystal decay curve and find $1/\Gamma$. For acquisitions (a) and (b), we found $1/\Gamma_P = 1.5$ ns in both cases, and respectively $1/\Gamma = 20.5$ and 5 ns and $B_P/B_0 = 0.63$ and 0.5.

Eventually, the theoretical formula for $c(\tau)$ is plotted on figure 2 with the parameters measured above. An excellent agreement is found with the measured correlation function, confirming the hypothesis of single-photon emission from the nanocrystal.